TWENTYFIFTH EUROPEAN ROTORCRAFT FORUM

Paper n° G8

ROTARY WING AEROELASTICITY IN FORWARD FLIGHT WITH REFINED STRUCTURE MODELLING

BY

A. R. M. ALTMIKUS, B. BUCHTALA, S. WAGNER
INSTITUT FÜR AERODYNAMIK UND GASDYNAMIK,
UNIVERSITÄT STUTTGART, GERMANY

SEPTEMBER 14-16, 1999
ROME
ITALY

ASSOCIAZIONE INDUSTRIE PER L'AEROSPAZIO, I SISITEMI E LA DIFESA
ASSOCIAZIONE ITALIANA DI AERONAUTICA ED ASTRONAUTICA

ROTARY WING AEROELASTICITY IN FORWARD FLIGHT WITH REFINED STRUCTURE MODELLING

A. R. M. Altmikus, B. Buchtala and S. Wagner
Institut für Aerodynamik und Gasdynamik, Universität Stuttgart
Pfaffenwaldring 21, 70550 Stuttgart, Germany

1 Abstract

A modular approach for the numerical simulation of the aeroelastic behaviour of a multi-bladed helicopter rotor in forward flight is presented. For this purpose a new dynamic finite element model of the beam-like blade structure, DYNROT, is coupled with a three-dimensional finite volume Euler solver for unsteady compressible flows, INROT.

The Euler solver uses third order upwind discretization in the computational space for the convective terms and is second order accurate in time by using three point backward differences. Arbitrary, relative blade motion in the rotor reference system is enabled due to Chimera technique.

The dynamic behaviour of the various blades is simulated by a quasi one-dimensional Finite Element Method (FEM) using Timoshenko's beam theory. The dynamic blade model comprises calculation of coupled flap lag motion as well as coupled flap torsion. Blade deflections are directly solved in time by integrating the second order linear system of differential equations with the generalized-α algorithm.

The solution of the surface coupled two-field problem is found by the use of a staggered time-marching procedure. This procedure together with geometric conservative deformation of grids guarantees the high order accuracy of the overall method.

This new approach for simulation of blade dynamics is validated on experimental data achieved in flight tests with a *HUGHES-500* helicopter. Additionally it is compared with another method to describe the blade deformation, SIMPACK, which is based upon modal synthesis of the first natural modes of an Euler-Bernoulli beam model.

2 Introduction

The introduction of hingeless rotor blades to the helicopter has lead to improvements in important areas. The weight of the main rotor was reduced as well as its mechanical complexity leading to a decrease in maintenance expenditures and lower operational costs. Drawback was a risen vibration level due to momentum afflicted blade connection of hingeless blades. Vibration is considered a severe disadvantage with respect to passenger comfort and fatigue failure. This phenomenon is strongly determined by the aeroelastic interaction of the blade structure and the surrounding compressible, viscous flow.

In course of the development of suitable countermeasures, their efficiency within this interactive environment is examined with numerical simulation methods. Since the involved mechanisms take place in rather small scales referred to blade-length the correctness and reliability of results are highly dependent on the local accuracy of the applied simulation methods.

Modern aerodynamic methods inherently provide the demanded local accuracy but dependent on the underlying model equations, they are neglecting important physical properties of the rotor flow, which is charactarized by high instationarity, compressibility as well as viscosity. Today's Euler methods for inviscid rotor flows are widely used for simulation purposes and Navier-Stokes methods are under development.

The dynamic behaviour of rotor blades can be calculated with multiple rigid-body systems, finite beam elements, as well as shell elements and fully three dimensional finite elements. Nevertheless, a rotor blade can be regarded as a slender body, so that a beam-like representation serves as a sufficiently accurate simulation basis.

Recent research dealing with fluid-structure-coupling emphasises the importance of the fact that both, aerodynamic and structural model have to be thoroughly in tune with each other with, respect to spatial and time-wise discretization in order to simulate the observed aeroelastic phenomena.

3 Applied Solution Methods

3.1 Structure Dynamics

Physical Structure Model

The dynamic blade deformation is analyzed with the structure model DYNROT, which is based on a quasi one-dimensional finite element representation of a beam-like structure using Timoshenko's beam theory. In difference to Euler's beam theory, where cross-sections of the beam keep a perpendicular orientation to the bending axis, Timoshenko introduced shear deformation, thus allowing for an angle between tangential bending and cross-sectional normal direction. This model also accounts for rotational inertia.

Within the cross-section, tension centre [T] or shear centre [S] must not necessarily coincide with the centre of gravity [G]. Thus torsion and bending as well as axial strain and bending deformations are structure-sidedly coupled. Beyond that, the aerodynamic centre, i.e. the quarter chord line [Q], may have an offset to the other axes, thus allowing an aerodynamic coupling of the torsional and bending degrees of freedom.

The resulting differential equation for deflection of a simple fixed beam is of hyperbolic type, describing the transport of wave energy within the beam in a physically correct manner. Additionally, normal dispersion of wave velocities is ascertained [17] by Timoshenko's model.

The governing system of equations for the rotating beam was derived in the following way. The physical representation of the quasi one-dimensional beam is built up from infinitesimal thin cross-sectional layers. The deflection of each rigid slice is now formulated for its centre of gravity, relative to the undeformed centre of gravity line of the beam. The deflection is described by three rotational degrees of freedom and three translational degrees of freedom (Figure 1), subsumed in vector φ and vector $\boldsymbol{u}$.

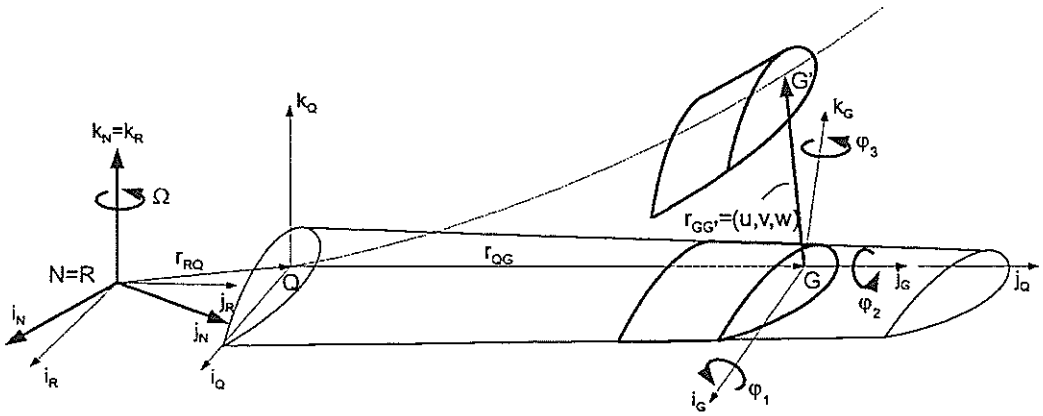

Figure 1: Finite element model of the rotor blade

Having a vector from the origin of the non-rotating reference frame [N] to the location of the centre of gravity [G'] in the deformed state of the beam, the corresponding velocities can be derived. With those entities, kinetic and potential energy of the cross-section can be formulated as length-related energy density functions in coordinates of the rotating reference system [R]. The energy terms can be further divided in translational and rotational kinetic energy and in elastic and gravitational

potential energy.

$$l = e_k - e_p = \frac{1}{2}(\rho A \dot{u}\dot{u} + \frac{1}{2}\omega\Theta\omega + EA\check{u}_{2B}^2 + \gamma^T G\gamma + \check{\varphi}^T T\check{\varphi} + N^0(\varphi_1^2 + \varphi_3^2)) + \rho A u g_{(R)} \quad (1)$$

Θ means the matrix of rotational inertias, G the matrix of shear stiffnesses and T the matrix of bending and polar stiffnesses. With

$$\check{u}_{2T} = \check{u}_2 - (z_{GT}\,\varphi_1)^{\check{}} + (x_{GT}\,\varphi_3)^{\check{}} \quad (2)$$

the spatial derivative ($\check{}$) of the axial strain deformation in the tension centre is yielded as a function of the DOF's. x_{GT} and z_{GT} are the distances between [G] and [T]. Timoshenko's theory delivers the shear angles as follows, with x_{GS} and z_{GS} as offsets of [S] from [G]:

$$\begin{aligned}\gamma_1 &= \check{u}_1 + \varphi_3 + (z_{GS}\,\varphi_2)^{\check{}} \\ \gamma_3 &= \check{u}_3 - \varphi_1 - (x_{GS}\,\varphi_2)^{\check{}}\end{aligned} \quad (3)$$

Dissipative energy is neglected in the first place but will be introduced later on by the mass and stiffness proportional Rayleigh-damping. Finally, N^0 represents the centrifugal force at the cross-section, which increases the elastic stiffness of the beam and causes an additional energy term in case of a rotating beam.

The complete Lagrange density function is obtained in dependence of time, radial position and generalized DOF's $q = (u, \varphi)^T = f(y,t)$, which are themselves a function of time and location along the beam axis

$$l = f(y, t, q, \check{q}, \dot{q}) \quad (4)$$

Assumed that the functional dependency of radial position is know, integration over beam length can be carried out for the Lagrange density so that the Lagrange function L is yielded. Further, nonconservative loads such as distributed aerodynamic forces acting on the system are written as virtual work. By Hamilton's principle the variation calculus of the time integral can be executed

$$\delta\mathcal{I} = \delta \int_{t=t_a}^{t_e} L\,Dt + \int_{t=t_a}^{t_e} \delta A\,Dt = 0 \quad (5)$$

so that the inhomogeneous system of differential is obtained:

$$\frac{D}{Dt}\frac{\partial L}{\partial \dot{q}} - \frac{\partial L}{\partial q} = F \quad (6)$$

Numerical Method

The previous formulation for the displacements is continuous in time and (1D) space. Only some rare problems can be fed into an analytical solution. For most arbitrary cases, solutions have to be found approximatively. Therefore the time and space dependent functions for the displacements are noted in a separation formulation as sum over finite elements

$$q(y,t) \approx \sum_{n=1}^{n_{el}} \left(h(y)_A\,\hat{q}(t)_A + h(y)_B\,\hat{q}(t)_B\right)_n \quad (7)$$

where $h(y)$ is only dependent on space and $\hat{q}(t)$ is only dependent on time. The nodal functions $\hat{q}$ serve as weighting functions for the normed form functions h and deliver the absolute amount of deformation at the element nodes. The functions h determine the form or devolution of the displacement within the element. These spatial functions were chosen linear over the element although there are proposals for

higher order Timoshenko beam elements [23, 7]. Since the fine spatial discretization of the aerodynamic grid will be used for the structure as well, linear functions turned out to be sufficiently accurate for the discussed problem. The negative side effect of shear locking is circumvented by reduced integration.

The finite element formulation is now introduced into the Lagrange density function. After spatial integration over the beam axis variation is performed for the whole equation. Thus leading to a linear system of ordinary differential equations

$$\boldsymbol{M}\ddot{\boldsymbol{Q}} + \boldsymbol{D}\dot{\boldsymbol{Q}} + \boldsymbol{K}\boldsymbol{Q} = \boldsymbol{G} + \boldsymbol{F}^{rot} + \boldsymbol{F} + \boldsymbol{M}^{c}\ddot{\boldsymbol{Q}}^{c} + \boldsymbol{D}^{c}\dot{\boldsymbol{Q}}^{c} + \boldsymbol{K}^{c}\boldsymbol{Q}^{c} = \boldsymbol{F}^{RHS} \tag{8}$$

$\boldsymbol{M}^c$, $\boldsymbol{D}^c$ and $\boldsymbol{K}^c$ are the coefficient matrices of the forced DOF movements, whereas $\ddot{\boldsymbol{Q}}^c$, $\dot{\boldsymbol{Q}}^c$ and $\boldsymbol{Q}^c$ are the accompanying column vectors of the time dependent constraints. Through such constraints cyclic and collective pitch as well as pre-cone and pre-lag are introduced.

This ODE-system is integrated in time by a generalized-α method presented by Chung and Hulbert [4]. This algorithm provides an optimal combination of high frequency and low frequency dissipation. It is implicit, unconditionally stable and of second-order accuracy. By appropriate choice of the underlying parameters it can be transfered into other α-methods like the Hilber-Hughes-Taylor or the Newmark algorithm. It can be further degraded with respect to frequency damping and phase error characteristics into the midpoint rule which still is second-order time-accurate.

3.2 Rotary Wing Aerodynamics

Physical Fluid Model

The three-dimensional, unsteady Euler equations are used to analyse the flow field around the helicopter rotor. They are formulated in a hub attached, non inertial rotating frame of reference with explicit contributions of centrifugal and Coriolis forces.

The computational grid of a rotor blade is supposed to have an arbitrary motion relative to the rotating frame of reference. This is due to the cyclic pitch control as well as to the actual blade degrees of freedom. Thus, the Euler equations are formulated using time invariant body fitted coordinates [2, 21]:

$$\frac{\partial \boldsymbol{\phi}}{\partial \tau} + \frac{\partial \boldsymbol{e}}{\partial \xi} + \frac{\partial \boldsymbol{f}}{\partial \eta} + \frac{\partial \boldsymbol{g}}{\partial \zeta} = \boldsymbol{k} \tag{9}$$

This so-called arbitrary Lagrangian-Eulerian (ALE) formulation allows each grid point to move with a distinct velocity in physical space, relative to the rotating reference system. The vector of the conservative variables, multiplied by the cell volume, is given by

$$\boldsymbol{\phi} = V \cdot (\rho, \rho\bar{u}, \rho\bar{v}, \rho\bar{w}, \bar{\bar{e}}) \tag{10}$$

Here the velocity and energy are given in terms of absolute quantities. Krämer [14] showed that using absolute quantities obviates systematic numerical errors and therefore preserves uniform flow when using a rotating frame of reference. The flux vector components of $\boldsymbol{e}$, $\boldsymbol{f}$, and $\boldsymbol{g}$ as well as the force vector $\boldsymbol{k}$ can be found in [21, 25].

For the finite volume cell-centred scheme, the flow variables are assumed to be constant within the cell. Since their values undergo a variation throughout the flow field, discontinuities arise at the cell boundaries. The evaluation of the fluxes at the cell faces is done by an approximate Riemann solver developed by Eberle [6]. The uniformly high order non-oscillatory (UNO) scheme [10] is used for the spatial discretization.

Geometric Conservation Law

Several sources [22], [5], [26], [15] point out, that the five conservation equations for mass, moment and energy on a moving grid does not automatically lead to a consistent approximation of the fluid flow,

because another numerical scheme – the "geometric conservation law" (GCL) – may not be fulfilled. This additional condition was incorporated in INROT by Hierholz [12], [11]. It is the conservation equation for the cell volume and states, that the volume change per time must equal the volume flux due to the moving cell boundaries. In time invariant body fitted coordinates it reads

$$\frac{\partial V}{\partial \tau} + \frac{\partial u_g}{\partial \xi} + \frac{\partial v_g}{\partial \eta} + \frac{\partial w_g}{\partial \zeta} = 0 \tag{11}$$

Here, V means the cell volume and $\boldsymbol{v}_g = (u_g, v_g, w_g)^T$ the grid velocity.

Since the cell volumes V are known geometric values, solely the grid velocities are the remaining entities to fulfill the GCL. Now it becomes clear, that the simple choice of grid deformation velocities which stem from external structure mechanic models might not determine the cell face velocities in a satisfying manner. But even these velocities can be obtained in a theoretically justified way if they are constructed with the known grid point positions at the actual and some former time steps.

Wake Capturing with Chimera Technique

The comprehensive simulation of multi-bladed rotors in forward flight has to take into account the reciprocal influence of the blades. The various blades affect themselves through their wakes, generated when lift is produced. Especially in flight situations with little down-wash like low-speed level flight or descend flight the rotor blades strongly interact with their own wake system. In such cases the distinct vortices of the flow field have to be resolved.

One possible approach is to implicitly capture the wake of a helicopter rotor by use of a sufficiently large computational domain which is able to resolve and transport the complete wake without further modelling. A separate grid is wrapped around each rotor blade. The individual blade grids are placed inside a base grid which covers the entire computational domain. The embedded grids exchange information at their boundaries with the base grid and hence with each other. Figure 2 shows the grid configuration of a five-bladed *Hughes 500* helicopter rotor.

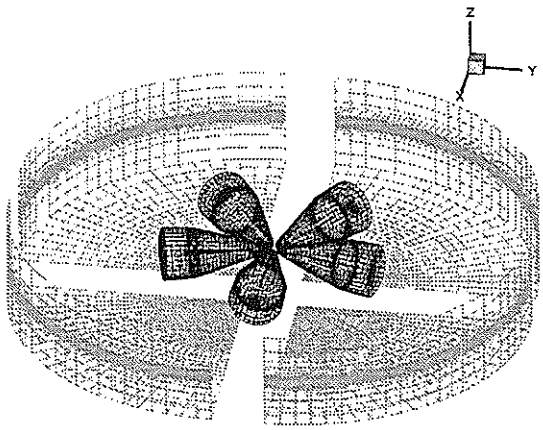

Figure 2: Chimera grids

The Chimera technique was incorporated in the flow solver INROT by Stangl [21]. Due to the large number of grid-points the computing time increases accordingly. Furthermore, additional time is needed for the search of transfer cells in the various grids. In order to minimize the required computing time, INROT was parallelized for shared memory architectures [25]. Each of the grids shown in Figure 2 is assigned to a processor. In order to achieve a good load balancing the base grid is divided into separate blocks, each with approximately the same number of grid points as the blade grids.

4 Fluid Structure Coupling

In very simple and small-scale structural problems the coupled system can be solved in a way that combines the fluid and structural equations of motion into one single formulation. This monolithic set of differential equations describes the fully coupled fluid structure system as a unity. However, we have to deal with the nonlinear Euler equations. The governing equations for the structure may be linear or non linear. It has been pointed out in [15] that the simultaneous solution of these equations by a monolithic scheme is in general computationally challenging, mathematically suboptimal and from the point of software development unmanageable.

Alternatively, the fluid structure coupling can be accomplished by partitioned procedures [3], [8], [15], [18]-[20], [24]. The fluid and structure partitions are processed by different programs with interactions only due to external input of boundary conditions, provided at synchronisation points. In the meantime the fluid and the structure evolves independently, each one of them using the most appropriate solution technique. This approach offers several appealing features, including the ability to use well-established solution methods within each discipline, simplification of software development efforts, and preservation of software modularity.

The exchange of boundary conditions – surface forces to the structural code and blade motion to the fluid solver – is best done consistent within the integration schemes used. Therefore, integrating from time level t^n to t^{n+1}, the implicit flow solver INROT is provided with boundary conditions at time level t^{n+1}. The implicit dynamic solver DYNROT obtains exchange data from time level t^{n+1} as well, but updates the structure consistently with a half time-step positive offset from $t^{n+1/2}$ to $t^{n+3/2}$. This is done by applying the above mentioned time integration method transforming it by appropriate parameter choice into the midpoint rule. An advantage of the midpoint rule is, that it allows the consistent construction, and not just the extrapolation of the structure displacement q at t^{n+1} with the structure state $Q = (q, \dot{q})^T$ at $t^{n+1/2}$

$$q^{n+3/2} = q^{n+1/2} + \frac{\Delta t}{2}(\dot{q}^{n+1/2} + \dot{q}^{n+3/2}) \tag{12}$$

$$\Longleftrightarrow \quad q^{n+3/2} - \frac{\Delta t}{2}\dot{q}^{n+3/2} = q^{n+1/2} + \frac{\Delta t}{2}\dot{q}^{n+1/2} \equiv q^{n+1}$$

Piperno proved in [19] that the inconsistent treatment of boundary conditions reduces the accuracy of the coupled system and eventually deteriorates the stability limit. Following his methodology Hierholz showed in [11] that 2nd order accuracy in time is maintained for the complete aeroelastic method using the depicted implicit-implicit staggered procedure.

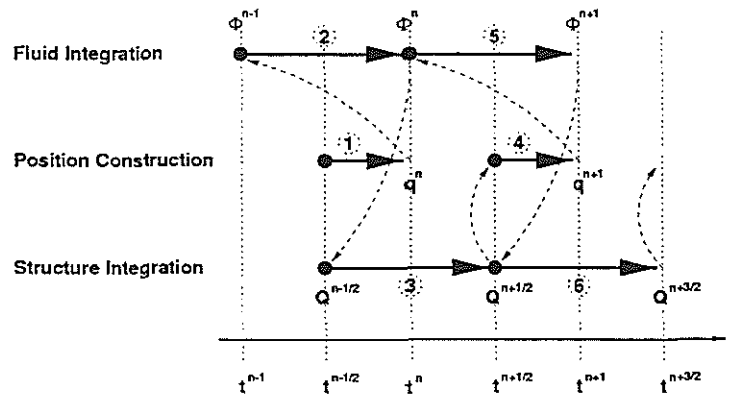

Figure 3: Implicit-implicit partitioned procedure

5 Results

5.1 Validation of Structure Method

The structure model was validated on numerous test cases. One shall be presented here, which is especially suited for rotor blade calculations. This test case described by Harris [9] gives an analytical function for the rotor flap bending deflection at realistic forward flight conditions and satisfies the boundary conditions of a pinned free beam. It is dependent on the azimuthal position of the blade and the radial position on the blade. This function is inserted in the governing differential equation for flap-wise bending of a rotating beam (e.g. see [13]) and the correlated aerodynamic force distribution is analytically derived.

Equivalently, the deflection function can be inserted into the differential equation for lag-wise bending [13]:

$$\rho A\ddot{u}_1 + EI_{33}\overset{\text{IV}}{\breve{u}}_1 - \frac{1}{2}\rho A\omega^2(R^2 - y^2)\breve{u}_1 + \rho A\omega^2 y\breve{u}_1 - \rho A\omega^2 u_1 = p_1 \tag{13}$$

As the given function for the blade deflection represents a pinned free beam, Coriolis forces would agitate rigid body motion about the lag hinge during simulation. Thus, as the numerical solution evolves during the calculation, it would be no longer comparable to the analytical solution. Therefore an analogous function was built up in order to conform with the boundary conditions of a fixed free beam. This was done by simply dropping the first order radial terms of the amplitude functions of the harmonic series given by Harris, obtaining:

$$\begin{aligned}
\frac{u_1}{R} &= f(\psi, Y) = f(\psi, \frac{y}{R}) \\
&= \cos(0\psi)\left(-\frac{4}{45}Y^{10} + \frac{8}{55}Y^{11} - \frac{2}{33}Y^{12}\right) \\
&+ \cos(1\psi)\left(+\frac{9}{160}Y^5 - \frac{3}{40}Y^6 + \frac{3}{112}Y^7\right) \quad + \sin(1\psi)\left(-\frac{1}{15}Y^5 + \frac{4}{45}Y^6 - \frac{2}{63}Y^7\right) \\
&+ \cos(2\psi)\left(-\frac{1}{30}Y^7 + \frac{1}{20}Y^8 - \frac{7}{360}Y^9\right) \quad + \sin(2\psi)\left(+\frac{1}{40}Y^5 - \frac{1}{30}Y^6 + \frac{1}{84}Y^7\right) \\
&+ \cos(3\psi)\left(-\frac{1}{108}Y^{10} + \frac{1}{66}Y^{11} - \frac{5}{792}Y^{12}\right) \quad + \sin(3\psi)\left(+\frac{1}{32}Y^8 - \frac{7}{144}Y^9 + \frac{7}{360}Y^{10}\right) \\
&+ \cos(4\psi)\left(-\frac{7}{330}Y^{11} + \frac{7}{198}Y^{12} - \frac{7}{468}Y^{13}\right)
\end{aligned} \tag{14}$$

Of course this test case is no longer related to real experiments but serves the purpose of verifying the inplane calculations of the structure code quite well. In consequence the derived analytic function of the resulting external load p_1 for the lagging-case is not a representation of any physical aerodynamic load either.

The underlying differential equations for lag bending and flap bending are based on an Euler beam. Otherwise the presented FEM falls back upon Timoshenko's beam theory. But the blade can be considered as slender so that the differences between both models are expected to be minimal in this case. Figures 4 and 5 confirm that assumption and further prove the accuracy of the structural model.

5.2 Hughes 500: Simulation versus Flight Test

A fully coupled aeroelastic simulation with both methods exchanging the determining boundary conditions at their common physical border, the blade surface, was compared against flight test results. These were gained by Lindert and described in [16]. In particular two measurements on the *Hughes 500* helicopter were chosen for comparison: a hover flight and a 100kt forward flight.

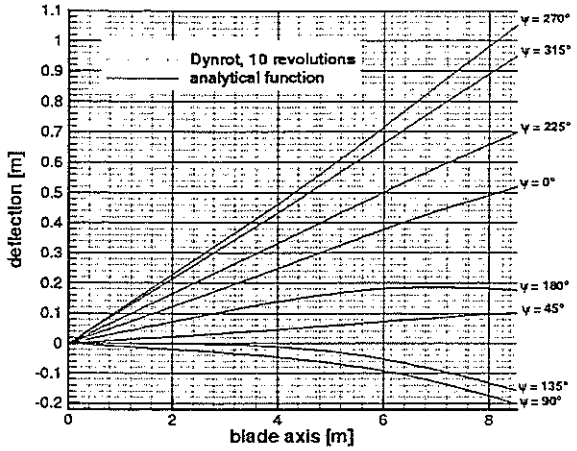

Figure 4: Analytical and numerical flap deflection

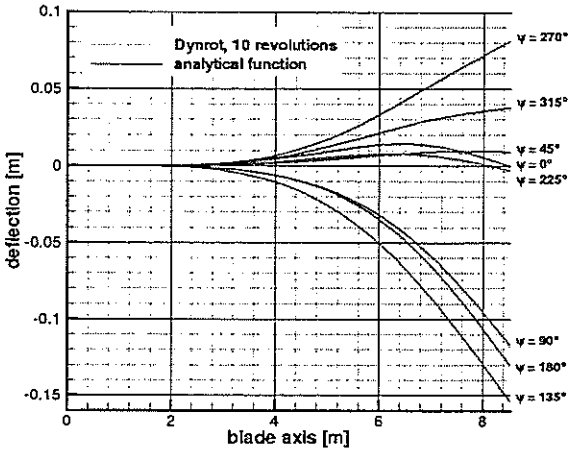

Figure 5: Analytical and numerical lag deflection

For this aeroelastic simulation the isolated rotor was considered fixed in space similar to a wind tunnel situation. The five-bladed Chimera grid system, depicted in figure 2, was used. 49 exchange points were used along thecentre of gravity line [G] of the blade matching the grid point distribution as well as the position of the structure nodes. Thus, any interpolation of boundary conditions was avoided.

The structure model was set up accounting for the special hinge construction of the *Hughes 500* rotor. Here the main rotor blades are connected to the rotor hub by a ball joint. Strap packs carry the centrifugal forces at the hinge, give the necessary high bending stiffness in lag direction and allow an unconfined flap movement. The blade has a rectangular shape and is equipped with a NACA 0015 profile of $0.18m$ chord length. It is linear twisted by $-9°$ and has an overall length of $3.5m$. The relevant parameter of both flight states are summarized in the following table:

		hover	forward flight
rotor radius	$[m]$	4.05	4.05
rotational speed	$[rad/s]$	51.836	51.836
helicopter velocity	$[kt]$	0	100
rotor advance ratio	$[-]$	0	0.25
speed of sound	$[m/s]$	340.4	340.4
rotor shaft angle	$[°]$	0	-4.0

Table 1: Parameter of both test cases

Measurements during this test campaign comprised flap angle β about the hinge but no control angles for collective and cyclic pitch. Therefore these had to be determined by a trim calculation, trimming for the observed flap angle. For the hover case the collective pitch angle has been used as trim parameter, to obtain a flap angle matching with the measured one. In case of the forward flight the triple of collective and both cyclic pitch angles has been trimmed to meet the measured flap angle considered approximately harmonic. The yielded values have been listed in table 2.

In the following the numerical simulations were confronted with the measurements. Additionally the results obtained with the previously described FEM DYNROT are compared with results which were delivered by Hierholz [12] who used the structure code SIMPACK. The latter method is based upon a multi-body-method where the dynamic system is composed of single rigid or elastic bodies,

		hover	forward flight
ϑ_0	[°]	7.3	8.33
ϑ_c	[°]	0.0	1.17
ϑ_s	[°]	0.0	−7.31

Table 2: Trimmed control angles

which are connected via joints. A modal formulation is used for the bending degrees of freedom of the blade which is approximated by a Euler-Bernoulli beam. The DOF's are structure-wise decoupled and torsion is neglected. For lag motion and flap motion the three first elastic modes are used. The rigid body motion about the flap hinge is represented by an additional rigid body mode. The linear system of ODEs is integrated in time by the Newton Method which is explicit and of first order accuracy.

5.2.1 Hover

For the hover test case the span-wise load distribution is presented in figure 6 and the elastic flap deformation is depicted in figure 7. Both are in pretty good agreement with the flight test measurements if one bears in mind, that first during a hover flight in opposite to a wind tunel situation a true steady flight condition can not be attained. Therefore the measurement data has been averaged over the azimuth. Second, air loads have not been gained by recording pressure values. Instead absolute forces have been reconstructed out of measured structural deformation and distributed loads have been derived under the assumption of piece-wise constant loads.

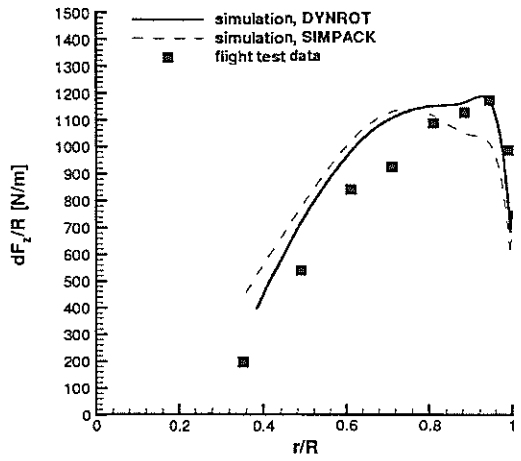

Figure 6: Distributed loads in hover

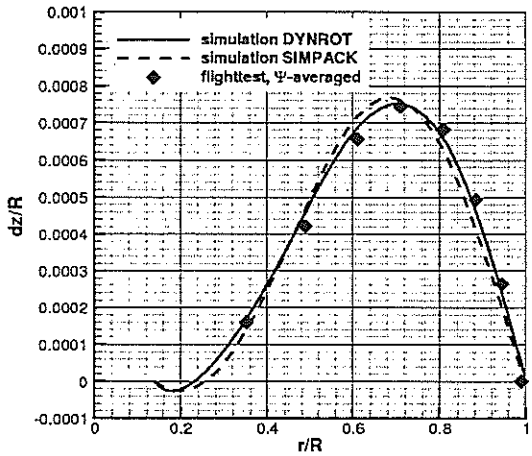

Figure 7: Flap bending deformation in hover

The flap deflection is slightly better represented by the DYNROT calculations. This is due to the included torsional degrees of freedom. A negative torsional moment which is caused by the dynamics of the rotating blade reduces the incidence angle along the blade thus reducing the lift forces especially at the outer diameters and allowing the centrifugal forces to curve the blade a little more.

5.2.2 Forward Flight

For the 100kt forward flight some elastic deformations of flap bending at various azimuth angles can be found in figure 8. Speaking of the elastic deformation a congruence of curvatures with flight test data could not be totally fulfilled. But the results obtained with DYNROT are better than those obtained

with SIMPACK. This is again related to the torsional degrees of freedom. Especially the form of the bending curve towards the blade tip at $\Psi = 315°$ proves that fact, although the line is quantitatively seen quite far away from the measurement values.

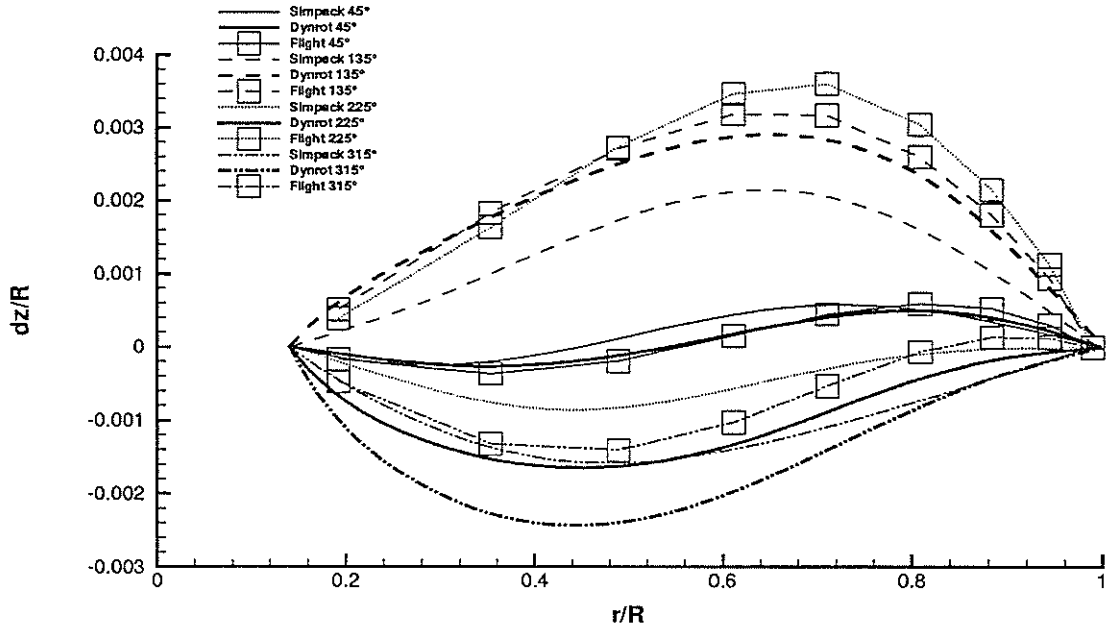

Figure 8: Flap bending deformation in forward flight

Generally, a direct comparison of isolated rotor simulation and flight test data for forward flight has to be handled with utmost care. First, a flight test does not guarantee a precise and well defined test environment as a wind tunnel does. Second, isolated rotor simulations neglect all occurring interaction of rotor flow with the fuselage and tail boom situated underneath.

Some other reasons concern this special test case. On the one hand the rotor shaft angle has not been measured during the flight test. Thus, a more or less reasonable value of $-4°$ had to be estimated. On the other hand the structure model has not been described precisely enough with respect to elastic properties of the blade like moments of inertia and offsets between the relevant axises. Furthermore, eigenfrequencies have only been given for flap bending but not for torsion or lag bending mode shapes. Here some assumptions had to be made as well, in order to construct a consistent structure model. The used properties are presented in table 3.

density	ρ	$[kg/m^3]$	2787.0
sectional area	A	$[m^2]$	$12.3 \cdot 10^{-4}$
Young's modulus	E	$[N/m^2]$	$7.31 \cdot 10^{10}$
shear modulus	G	$[N/m^2]$	$2.50 \cdot 10^{10}$
flap moment of inertia	I_x	$[Nm^2]$	$5.50 \cdot 10^{-8}$
polar moment of inertia	I_t	$[Nm^2]$	$2.68 \cdot 10^{-6}$
lag moment of inertia	I_z	$[Nm^2]$	$2.62 \cdot 10^{-6}$
axis distances from [Q]	x_G, x_S, x_T	$[m]$	0.0

Table 3: Structural properties

6 Conclusions

We presented a simulation method for the aeroelastic analysis of helicopter rotors. It allows to solve the highly demanding task of coupled aeroelastic calculation for any complex layout of multi-bladed helicopter rotors with arbitrary relative blade motion in a transonic, unsteady aerodynamic environment. A highly modular, partitioned approach could be realized using a time-marching staggered coupling scheme.

For the structure dynamics a FEM for a quasi one-dimensional beam based on the Timoshenko's beam theory has been developed for rotating applications. This method is especially suited for aeroelastic calculations, because it offers the possibility to introduce offsets between the aeroelastically relevant axises. Furthermore it enables appropriate control input at arbitrary hinge positions. The underlying ODEs are integrated directly in time by an implicit method of second order.

The fluid domain is described by the Euler equations in an ALE formulation. A finite volume upwind flow solver is used to solve the equations numerically. Inside the aerodynamic computation relative blade motion is gathered with the incorporated chimera technique. With an efficient and robust algebraic three dimensional grid deformation algorithm the elastic deformation of the blades was tracked inside the fluid domain.

Calculations of the aeroelastic behaviour of the five-bladed *Hughes 500* rotor in hover and 100kt forward flight were shown. These included flap bending, lag bending and elastic blade torsion. The results were compared with flight test data and a second coupled method. The importance of including the torsional degrees of freedom has been clearly shown. Excellent agreement of calculation with presented method and the flight test experiments could be shown for hover.

Although the forward flight comparisons have to be carried out with caution, they show a good qualitative and quantitative accordance with the experiment. Finally it has to be pointed out that a most comprehensive descriptions of the structure as it is offered by this new method is superior to a less refined method.

References

[1] Altmikus, A. R. M.: *Dynamikberechnung eines elastischen Rotorblattes unter Verwendung der Timoshenko-Balken-Theorie.* Master Thesis, Institut für Statik und Dynamik der Luft- und Raumfahrtkonstruktionen, Universität Stuttgart, 1998.

[2] Brenneis, A.: *Berechnung instationärer zwei- und dreidimensionaler Strömungen um Tragflügel mittels eines impliziten Relaxationsverfahrens zur Lösung der Eulergleichungen.* Ph.D. Thesis, Institut für Luftfahrttechnik und Leichtbau, Universität der Bundeswehr München, Neubiberg, 1989.

[3] Buchtala, B., Wehr, D. and Wagner, S.: *Coupling of Aerodynamic and Dynamic Methods for the Calculation of Helicopter Rotors in Forward Flight.* 23rd European Rotorcraft Forum, pp. 5.1-5.12, Dresden, September 1997.

[4] Chung, J. and Hulber, G. M.: *A Time Integrateion Algorithm for Structural Dynamics With Improved Numerical Dissipation: The Generalized-α Method.* Journal of Applied Mechanics, vol. 60, pp. 371-375 June 1993.

[5] Demirdzic, I., Peric, M.: *Space Conservation Law in Finite Volume Calculations of Fluid Flow.* International Jounal for Numerical Methods in Fluids, vol. 8, 1037-1050, 1988.

[6] Eberle, A.: *MBB-EUFLEX. A New Flux Extrapolation Scheme Solving the Euler Equations for Arbitrary 3-D Geometry and Speed.* Report MBB-LKE122-S-PUB-140, MBB, Ottobrunn, Germany, 1984.

[7] Friedman, Z. and Kosmatka, J. B.: *An Improved Two-Node Timoshenko Beam Finite Element.* Computers & Structures, vol. 47, no. 3, pp. 473-481, 1993.

[8] Guruswamy, G.P.: *Time-Accurate Unsteady Aerodynamic and Aeroelastic Calculations of Wings using Euler Equations.* AIAA paper 88-2281, 29th AIAA Structures, Structural Dynamics and Materials Conference, Williamsburg, Virginia, April 1988.

[9] Harris, F. D.: *The Rotor Blade Flap Bending Problem - An Analytical Test Case.* Technical Notes, Journal of the American Helicopter Society, pp. 64-67, October 1992.

[10] Harten, J. and Osher, S.: *Uniformly High-Order Nonoscillatory Schemes I.* SIAM Journal on Numerical Analysis, vol. 24, pp. 279-309, 1987.

[11] Hierholz, K.-H.: *Ein numerisches Verfahren zur Simulation der Strömungs-Struktur-Interaktion am Hubschrauberrotor.* Ph.-D. Thesis, Institut für Aerodynamik und Gasdynamik, Universität Stuttgart, 1999.

[12] Hierholz, K.-H. and Wagner, S.: *Simulation of Fluid Structure Interaction at the Helicopter Rotor.* Proceedings of the 21st ICAS Congress, Melboune, Australia, September 13-18, ICAS-98-2.9.4, 1998.

[13] Johnson, W.: *Helicopter Theory.* Princeton University Press, Princeton, New Jersey, 1980.

[14] Krämer, E.: *Theoretische Untersuchungen der stationären Rotorblattumströmung mit Hilfe eines Euler-Verfahrens.* Ph.D. Thesis, Institut für Luftfahrttechnik und Leichtbau, Universität der Bundeswehr München, Neubiberg, 1991.

[15] Lesoinne, M. and Farhat, C.: *Improved Staggered Algorithms for the Serial and Parallel Solution of Three-Dimensional Nonlinear Transient Aeroelastic Problems.* Fourth World Conference on Computational Mechanics, E. Onate and S.R. Idelsohn, editors, Barcelona, Spain, 1998.

[16] Lindert, H.-W.: *Anwendung einer strukturmechanischen Methode zur Rekonstruktion der Luftkräfte am rotierenden Rotorblatt aus Windkanal- und Flugversuchsmeßdaten.* Ph.D. Thesis, RWTH Aachen, VDI-Fortschrittsberichte, Reihe 12, Nr. 245, VDI Verlag, Düsseldorf, 1994.

[17] Nellessen, D. M.: *Schallnahe Strömungen um elastische Tragflügel.* Ph.D. Thesis, RWTH Aachen, VDI-Fortschrittsberichte, Reihe 7, Nr. 302, VDI Verlag, Düsseldorf, 1996.

[18] Park, K.C. and Felippa, C.A.: *Computational Methods for Transient Analysis.* In T. Belytschko and T.J.R. Hughes, editors, *Partitioned analysis of coupled systems*, pp. 157-219, North-Holland Pub. Co., 1983.

[19] Piperno, S., Farhat, C., and Larrouturou, B.: *Partitioned Procedures for the Transient Solution of Coupled Aeroelastic Problems, Part I: Model Problem, Theory and Two-Dimensional Application.* Computer Methods in Applied Mechanics and Engineering, vol. 124, no. 1-2, pp. 79-112, June 1995.

[20] Rausch, R.D., Batina, J.T., and Yang, T.Y.: *Euler Flutter Analysis of Airfoils using Unstructured Dynamic Meshes.* AIAA paper 89-13834, 30th AIAA Structures, Structural Dynamics and Materials Conference, Mobile, Alabama, April 1989.

[21] Stangl, R.: *Ein Eulerverfahren zur Berechnung der Strömung um einen Hubschrauber im Vorwärtsflug.* Ph.D. Thesis, Institut für Aero- und Gasdynamik, Universität Stuttgart, 1996.

[22] Thomas, P.D., Lombard, D.K.: *Geometric conservation law and its application to flow computations on moving grids.* AIAA Jourmal, vol. 17, pp. 1030-1037, 1979.

[23] Tessler, A. and Dong, S.B.: *On a Hierarchy of Conforming Timoshenko Beam Elements.* Computers & Structures, vol. 14, no. 3-4, pp. 335-344, Pergamon Press Ltd. 1981.

[24] Weeratunga, S.K. and Pramono, E.: *Direct Coupled Aeroelastic Analysis through Concurrent Implicit Time Integration on a Parallel Computer.* AIAA paper 94-1550, 35th AIAA Structures, Structural Dynamics and Materials Conference, Hilton Head, South Carolina, April 1994.

[25] Wehr, D.: *Untersuchungen zum Wirbeltransport bei der Simulation der instationären Umströmung von Mehrblattrotoren mittels der Eulergleichungen.* Ph.D. Thesis, Institut für Aero- und Gasdynamik, Universität Stuttgart, 1998.

[26] Zhang, H., Reggio, M., Trepanier, J.Y.: *Discrete Form of the GCL for Moving Meshes and Its Implementation in CFD Schemes.* Computers and Fluids, vol. 22, no. 1, pp. 9-23, 1993.